Inducing spin triplet superconductivity in a ferromagnet

Voltan, S.

5

COLOSSAL PROXIMITY EFFECT IN A SUPERCONDUCTING TRIPLET SPIN VALVE BASED ON THE HALF-METALLIC FERROMAGNET CrO_2

Superconducting triplet spin valves (TSVs) built by using a 100 % spin polarized half-metallic ferromagnet, such as CrO_2, are extremely efficient. The application of out-of-plane magnetic fields results in an a strong suppression of T_c, by well over a Kelvin. The observed effect is an order of magnitude larger than previous studies on TSVs with standard ferromagnets and is particularly important in view of the growing interest in generating long range triplet supercurrents for dissipationless spintronics.

Contents

Parts of this chapter have been published in:
A. Singh, S. Voltan, K. Lahabi, and J. Aarts. Colossal proximity effect in a superconducting triplet spin valve based on the half-metallic ferromagnet CrO_2. *Phys. Rev. X* **5**, 021019 (2015),
S. Voltan, A. Singh, and J. Aarts. Triplet generation and upper critical field in superconducting spin valves based on CrO_2, *Phys. Rev. B* **94**, 054503 (2016).

5.1 Introduction

As discussed in Chap.1 and 2, ferromagnets can sustain supercurrents through the formation of equal spin triplet Cooper pairs and the mechanism of odd-frequency pairing. Since such pairs are not broken by the exchange energy of the ferromagnet, superconducting triplet correlations are long-ranged and spin-polarized, with promises for superconducting spintronics devices [1–3]. In S/F hybrids the spin polarized triplet correlations can be generated by converting Cooper pairs from the singlet to triplet state via spin mixing and spin rotation at the S-F interface, which requires the presence of magnetic inhomogeneity [4–8]. Recently, it was shown that long range supercurrents could be engineered in S/F/S Josephson junctions by inserting an extra ferromagnetic layer between the superconductor and the central F-layer [9–12], in the configuration $S/F_1/F_2/F_1/S$. Still, quantitative understanding of the conversion process is mostly lacking since the spin activity of the interface is not a measurable parameter. Absolute values of the supercurrent are not easily predictable, which was illustrated clearly in a recent work of Klose *et al.* [13], where supercurrents in a Co-based Josephson junction could be increased more than an order of magnitude by manipulating the magnetization directions of F_1 and F_2. For acquiring such understanding, a Josephson junction has the disadvantage that it contains two sets of interfaces, which may not have the same amount of spin activity or even transparency. In this sense a TSV, pictorially sketched in Fig.5.1a, is a simpler device. It can be thought of as half of the Josephson junction, utilizing the same layer package $S/F_1/N/F_2$. The S-layer is chosen not too thick, so that the drainage of Cooper pairs through triplet conversion is reflected in the change of T_c of the stack, F_1 is thin in order to take part in the spin mixing, but not to break Cooper pairs, and F_2 is the drainage layer, which can be infinitely thick. N is added to magnetically decouple the ferromagnetic layers. By changing the relative magnetization directions of F_1 and F_2 the triplet pair generation is varied and thereby the amount of singlet pairs which is converted, making the operation a field-controlled proximity effect (see Sec.2.3.2). When F_1 and F_2 are orthogonal, triplet generation is maximum and T_c should be minimum. Therefore, the efficiency of a TSV can be gauged by the extent to which T_c decreases.

There are several recent experimental results on TSVs, which use standard ferromagnets (Fe, Co, Ni) and their alloys as spin mixers and drainage layers [14–18]. In all cases magnetic anisotropy or an antiferromagnetic pinning layer was used to reliably control the relative magnetization directions, always in the plane of the films. The maximum suppression of T_c achieved in such devices ranged from 120 mK (for a thin ballistic Co drainage layer) [15] to 20 mK (for diffusive TSVs) [14, 17, 18]. Our experi-

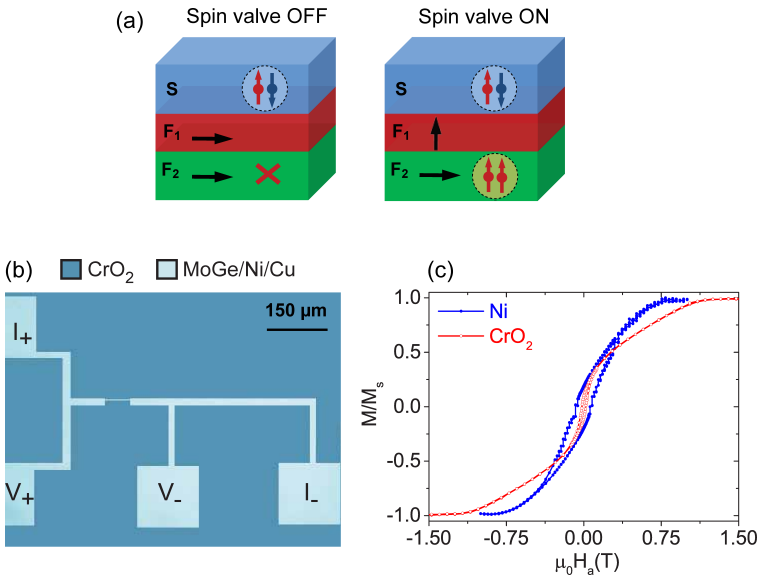

Figure 5.1: Device structure and magnetic characterization. (a) Working principle of a Triplet Spin Valve (TSV) with a half-metallic ferromagnet; the TSV is off (on) when the magnetizations of F_1 and F_2 are collinear (non-collinear), with a maximum effect when they are orthogonal. (b) Optical micrograph of a typical TSV where a MoGe(d_S)/Ni(1.5 nm)/Cu (5 nm) trilayer bridge of 10 μm width was patterned on a 100 nm thin film of CrO_2. (c) Magnetization hysteresis loops for CrO_2 (100 nm) and a multilayer (Ni(1.5 nm)/Cu(10 nm))$_{11}$/Ni(3 nm)/Cu(10 nm) measured with the magnetic field perpendicular to the sample plane. The magnetization M is normalised on the saturation magnetization M_S, which was 6.8×10^5 A/m for the CrO_2 film and 2.2×10^5 A/m for the Cu/Ni multilayer.

ments are different in two important aspects. One is the use of the half-metallic ferromagnet CrO_2 as the drainage layer. The other is that we vary the field from in-plane to out-of-plane. Unlike in-plane rotation of the field, out-of-plane rotation changes the critical field of the superconductor itself.

We therefore account for this by comparing our TSV with stacks where one of the F layers is absent, as well as with the simple S-layer. In this way we find that spin valve effects are present up to fields of Tesla's, and they are remarkably large, with a suppression in T_c as high as 1.6 K in 0.5 T (see Sec.5.3.1). The origin of this significant variation probably lies in the fact that CrO_2 is 100 % spin polarized and strongly supports triplet correlations. The triplet origin of the suppression in T_c is confirmed by the dependence of the TSV effect on the thickness of the mixer layer F_1. The non-monotonic behavior, presented in Sec.5.3.3, is indeed consistent with the model for triplet generation, which we discuss in Sec.2.3.2. In our devices the TSV efficiency is strongly determined by the interface transparency, in particular at the surface of CrO_2 where spin accumulation effects can occur. This will be discussed in Sec.5.3.2.

5.2 Experimental details

Our TSV is made of amorphous $Mo_{70}Ge_{30}$, Ni, Cu and CrO_2 as the S, F_1, N and F_2 layers, respectively. For simplicity $Mo_{70}Ge_{30}$ is called MoGe. An example of the investigated device is shown in the optical micrograph presented in Fig.5.1b: it consists of a 10 μm-wide MoGe/Ni/Cu trilayer bridge deposited on top of a CrO_2 film. Since CrO_2 is metastable at room temperature and atmospheric pressure, it cannot be prepared with conventional sputtering or evaporation techniques. High quality epitaxial CrO_2 thin films can be grown epitaxially by using chemical vapor deposition (CVD). The substrate used is TiO_2(100) because of its little lattice mismatch with CrO_2, only 3.79 % along the b-axis and 1.48 % along the c-axis [19]. Before the deposition the substrate is pretreated with Hydrofluoric acid (HF) in order to enhance the strain and therefore improve the quality of the film. The CVD process is done in a two-zone furnace, which is sketched in Fig.5.2. In one zone the substrate is kept at 390 °C and in the other zone the precursor (CrO_3) is heated to 260 °C. The precursor vapor is carried with O_2 gas (flow rate 100 sccm) to the substrate where it decomposes into CrO_2 over a very narrow temperature range (390-400 $°C$). CrO_2 selectively grows on TiO_2 in rectangular grains with the b-axis (010) and the c-axis (001) in plane. For bulk samples, the easy axis is expected to be along c. More details about the growth process and the properies of CrO_2 can be found in Ref. [21]. The MoGe/Ni/Cu trilayer

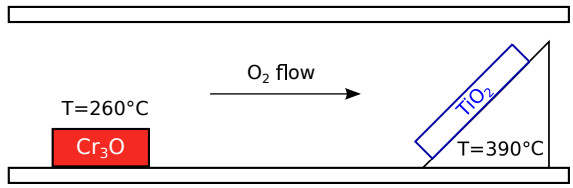

Figure 5.2: Schematic of the two-zone furnace used for the chemical vapor deposition (CVD) of CrO_2. On the left the CrO_3 precursor is at 260 °C while the TiO_2 substrate is heated to about 390 °*C*. The precursor vapor is carried with O_2 gas to the substrate where it decomposes into CrO_2. Adapted from Ref. [20].

bridge was deposited using sputtering and lift-off [22], aligned along the easy axis of CrO_2. Prior to the trilayer deposition, the top surface of CrO_2 was cleaned with an Argon ion plasma to remove the thin insulating Cr_2O_3 barrier which is prone to form at the end of the deposition process. Ar etching was performed in the sputter system used to deposit the Cu/Ni/MoGe stack by reversing the polarity of the plasma, using a pressure of 5×10^{-3} mbar and an RF power of 150 Watt. In this geometry, similar to the Josephson junction devices [12, 22, 23], the current is confined to the bridge only in the superconducting state. To characterize the magnetic properties of $F_{1,2}$ layers, their hysteresis loops (magnetization M versus applied field H_a) were measured using SQUID magnetometry in the out-of-plane configuration. Instead of a single Ni layer of 1.5 nm, we used a multilayer $(Ni(1.5)/Cu(10))_{11}/Ni(3)/Cu(10)$ in order to boost the signal (numbers in parentheses represent the thickness in nanometers). The data are given in Fig.5.1c and show that in both layers the rotation of the magnetization requires a field of order of a Tesla. For electrical measurements, devices were connected in a 4-probe geometry to a PPMS chip holder, which was loaded on a special rotator platform sample board for angle dependent magnetotransport measurements.

5.3 Results

5.3.1 Colossal triplet spin valve effect

For angle resolved magnetotransport measurements the magnetic field (H_a) was rotated in a plane normal to the sample. In this geometry, when $\theta = 0°$ the field is aligned with the current density (j), while $\theta = 90°$ corresponds to the

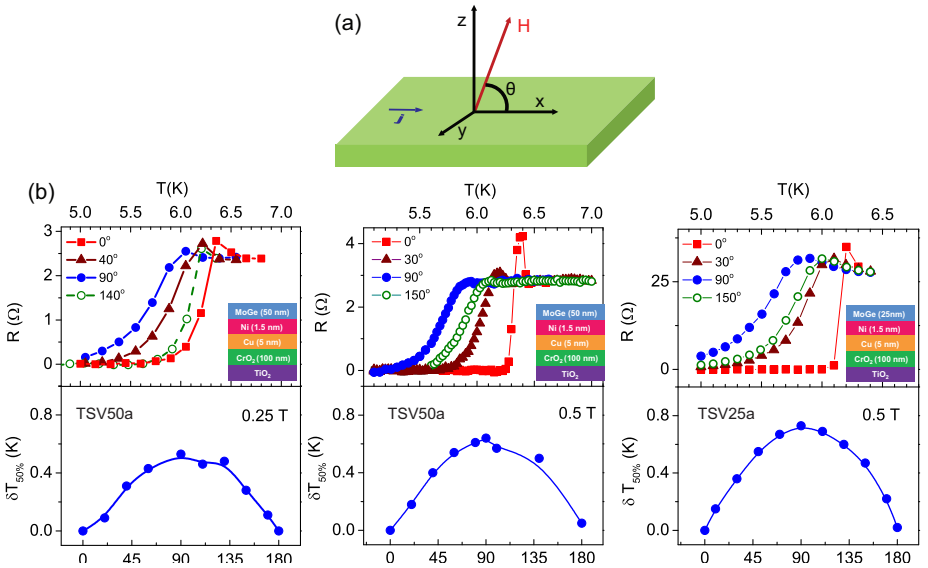

Figure 5.3: Colossal triplet spin valve effect. (a) Coordinate system used in angle dependent magnetotransport measurements, showing the direction of the current j, the applied field H_a and the angle θ between them. (b) Spin valve effect in the two spin valves MoGe(d_S)/Ni(1.5 nm)/Cu(5 nm)/CrO_2(100 nm) with d_S = 50 nm (TSV50a; left and middle), and d_S = 25 nm (TSV25a; right). Upper panels: resistive transitions for different θ as indicated. Lower panels: variation of $\delta T_{50\%} = T_{50\%}(0°)$ - $T_{50\%}(\theta)$ as a function of θ at 0.25 T (TSV50a) and 0.5 T (TSV50a, TSV25a), where $T_{50\%}$ is the temperature where the normal state resistance has decreased by 50 %. Note that a peak appears in the transition curves for measurements at $\theta = 0°$.

out-of-plane applied field, as outlined in Fig.5.3a. Fig.5.3b (upper panels) shows $R(T)$-curves at different angles of the magnetic field for two TSVs consisting of MoGe(d_S)/Ni(1.5)/Cu(5)/CrO_2(100), with two different values of the MoGe thickness i.e. d_S = 25 nm (called TSV25a[i]) and d_S = 50 nm (called TSV50a), and for fixed magnetic fields of 0.25 T and 0.5 T. We extract an operational parameter $T_{50\%}$ (for a discussion of this choice, see Appendix B) which is the temperature where the resistance has decreased to 50% of the normal resistance value. The variation of $T_{50\%}$ with θ is called $\delta T_{50\%} = T_{50\%}(0°)$ - $T_{50\%}(\theta)$. The lower panels show $\delta T_{50\%}$ as function of θ, and the curves clearly exhibit a maximum when the field is normal to the plane. Further points to note are: (i) the large values of the change, of about 550 mK and 650 mK for TSV50a in 0.25 T and 0.5 T, respectively, and 750 mK for TSV25a in 0.5 T; (ii) the significantly larger value of the normal state resistance for TSV25a; (iii) the sharp peak in

[i] In this chapter, TSV25 always refers to a TSV with d_S = 25 nm and TSV50 to a TSV with d_S = 50 nm.

resistance which in parallel field occurs at the onset of superconductivity and which smears out and disappears when rotating the field.

In order to discuss the first point we have to put the data in perspective. The superconductor itself will show a $T_{50\%}(\theta)$ variation, because the transition in parallel field is due to the onset of surface superconductivity, which is at a higher field (and temperature if the field is fixed) than the transition in perpendicular critical field. The change from surface to bulk effects also raises concerns about going from a vortex-free configuration to one where vortex flow may play a role. These issues are resolved by a straightforward comparison with the behavior of a single MoGe layer, for which we take a thickness of 50 nm. Stray fields of mixer and drainage layer may also play a role, and therefore we compare with devices of MoGe(50)/Ni(1.5)/Cu(5) and MoGe(50)/Cu(5)/CrO_2(100), as well. Fig.5.4a shows the transition curves of these devices at 0.25 T for in-plane (red squares) and out-of-plane (blue circles) configurations. All have comparable $\delta T_{50\%}$. In Fig.5.4b values of $\delta T_{50\%}$ for the different data sets are

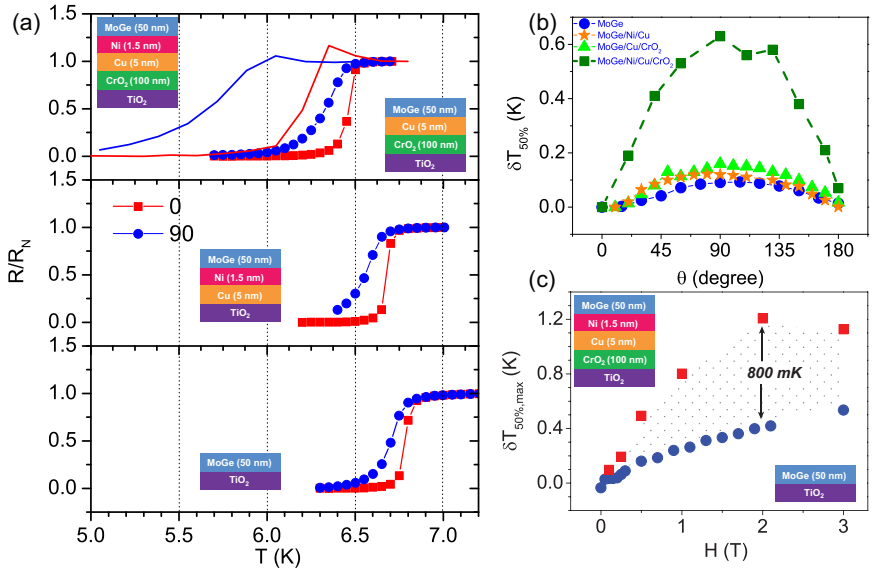

Figure 5.4: Non-triplet-generating layer combinations. (a) Transition curves for MoGe(50 nm)/Cu(5 nm)/CrO_2(100 nm) (top), MoGe(50 nm)/Ni(1.5 nm)/Cu(5 nm) (middle), and MoGe(50 nm) (bottom panel) for $\theta = 0°$ and $\theta = 90°$ at 0.25 T. The top panel also shows the results of the spin valve device TSV50a as drawn lines. (b) $\delta\ T_{50\%}$ as function of θ for these layered devices and for TSV50a at 0.25 T. (c) Variation of $T_{50\%,\max} = T_{50\%}(0°)$ - $T_{50\%}(90°)$ as function of applied field for MoGe(50) and TSV50b.

compared, again at a field of 0.25 T. It can be clearly seen that the variation in the TSV is significantly larger than in the other devices. Fig.5.4c shows the variation of $\delta T_{50\%,\max} = T_{50\%}(0°) - T_{50\%}(90°)$ as a function of the applied field for an isolated MoGe film and a TSV with a 50 nm MoGe layer called TSV50b. In both cases $\delta T_{50\%,\max}$ increases monotonically with the magnetic field up to 2 T. The shaded area in Fig.5.4c solely corresponds to the effect of triplet generation which can suppress $\delta T_{50\%,\max}$ by as much as 800 mK. We find TSV effects over a wide range of magnetic fields. This was not the case for previous TSVs measured in an in-plane configuration, where the maximum field of operation was limited to 0.2 – 0.3 T [18]. Robust proximity effects were also observed in CrO_2 based Josephson junctions [12, 22, 23] where critical currents in various configurations were observed up to the Tesla range. Slightly puzzling is that $\delta T_{50\%,\max}$ continues to increase well above the fields where saturation of both mixer and drainage layer have been achieved and both magnets are assumed to be collinear. We believe that this may be caused by the presence of non-collinear magnetic moments pinned at the CrO_2 interface. Noting that the difference between the TSV and the other stacks only lies in the insertion of an extra 1.5 nm layer of Ni, it seems reasonable to conclude that, just as in the case of the Josephson junctions, the Ni layer is instrumental in generating triplets. They are very efficiently drained by the CrO_2 layer which leads to the observed large spin valve effects.
Turning to the larger value of the normal state resistance R_N of TSV25a, as we will show in the next section, this can be used to probe the effects of the bare interface transparency, which is a critical parameter in determining the strength of proximity effect, and much studied in S/N and S/F hybrids [24, 25].

5.3.2 Interface transparency and spin accumulation

In our devices the transparency of the interface between the Cu/Ni/MoGe stack and the CrO_2 film is controlled by the Argon etching of the CrO_2 surface prior to the deposition of the other layers. The etching is a critical step in the fabrication, due to the fact that under-etching results in only partial removal of an unwanted Cr_2O_3 layer while over-etching induces disorder at the surface of CrO_2. Varying the Ar etching time allows to vary the interface transparency in a systematic manner. The transparency has a direct influence on the normal resistance of the device, which in essence consists of a top N-layer (MoGe) of high resistance and a bottom F-layer (CrO_2) of low resistance, with an interface resistance R_B in between. With contacts on top, R_B is in series with the low-resistance bottom layer and its measurable influence on R_N allows R_N to be used as a parameter for the interface transparency. Fig.5.5 shows the $R(T)$ transi-

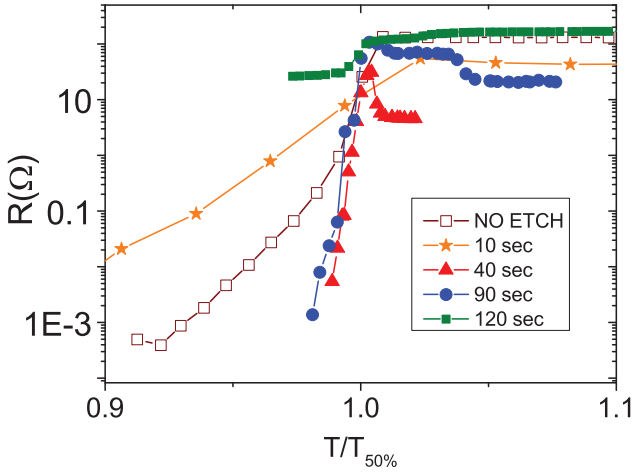

Figure 5.5: Resistive transitions for triplet spin valves TSV50 fabricated with various Ar etch times. The temperature T is normalized using $T_{50\%}$, the value where R has decreased to 50 % of the normal state value. Etch times are 0 sec ($T_{50\%}$ = 5.7 K, open square); 10 sec ($T_{50\%}$ = 3.4 K, filled star); 40 sec ($T_{50\%}$ = 6.4 K, filled triangle); and 120 sec ($T_{50\%}$ = 6.3 K, filled square).

tion curves on a logarithmic scale for R, of TSVs fabricated with different Ar etching times. The temperature axis is normalized by the value of $T_{50\%}$ for each curve. As expected, the etching time has a nonmonotonic influence on the normal resistance of a TSV. The TSV with no etching has a R_N value comparable to the one etched for 120 sec (overetching). Moreover, the value of 200 Ω is very close to the resistance of the MoGe/Cu/Ni bridge (measured to be 240 Ω) showing that without etching the interface resistance is very high, and the CrO_2 layer is effectively decoupled from the MoGe/Cu/Ni stack. For intermediate etching times R_N decreases, with a minimum value reached around 40 sec.

We take advantage of this by making different devices on the same CrO_2 film using different etching times. For this the film is covered with resist, a lift-off structure is written, the CrO_2 surface is etched for a certain amount of time, and the stack is deposited. This process is repeated with different etching times. Fig.5.6 depicts the effect of interface transparency on the performance of a TSV, characterized by $\delta T_{50\%}$. In Fig.5.6 we plot $\delta T_{50\%,max}$ against $1/R_N$ for the two sets of devices, TSV25 and TSV50, measured in 0.5 T (blue triangles and green circles) and a set TSV50 measured in 0.25 T (red squares). The devices TSV50a,b and TSV25a are plotted with special (open) sym-

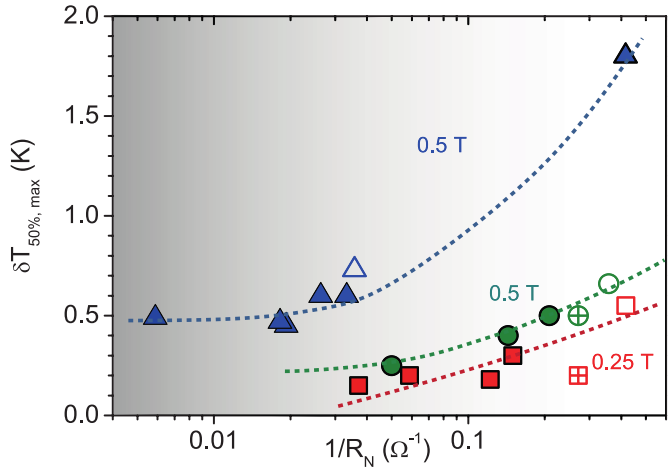

Figure 5.6: Dependence of TSV effect on interface transparency. Variation of $T_{50\%,\max}$ plotted against the inverse of the normal state resistance R_N (interface transparancy), for spin valve devices with different interfaces between the CrO_2 layer and the MoGe/Ni/Cu stack. Blue triangles: TSV25 (d_S = 25 nm), measured at 0.5 T; open symbol is TSV25a. Green circles (red squares): TSV50 (d_S = 50 nm), measured at 0.5 T (0.25 T). Symbols with + are device TSV50a, the open green circle (red square) is TSV50b.

bols. The performance of all TSVs increases monotonically with decreasing R_N, that is with increasing barrier transparency. Interface transparency also offers a natural explanation for the fact that TSV25 devices with higher R_N exhibit an effect comparable to the set TSV50. According to basic proximity effect theory, the thinner layer should show a stronger effect upon Cooper pair depletion, but as can be seen in Fig.5.6, this is counteracted by the lower interface transparency. In this respect it should also be remarked that the set TSV50 is surprisingly efficient when taking into account that the S-layer thickness is about ten times the superconducting coherence length ξ_S, which for MoGe is about 5 nm [26]. This again appears to be a consequence of the 100 % spin polarized ferromagnet.

Another striking feature in our results is the characteristic peak observed in several transition curves. In Fig.5.3b the peak, present at a finite in-plane field, is broadened and partially suppressed (or completely for TSV50a) when the field is rotated out-of-plane. For most of the measured TSVs with d_S = 50 nm the peak is not present at zero field, but then gradually appears by increasing the field. An example is given in Fig. 5.7a, for the structure TSV50a. For d_S = 25 nm, instead, the peak is often observed at zero field as well. This can be seen in Fig.5.7b, for TSV25-1.0 (1.0 indicates

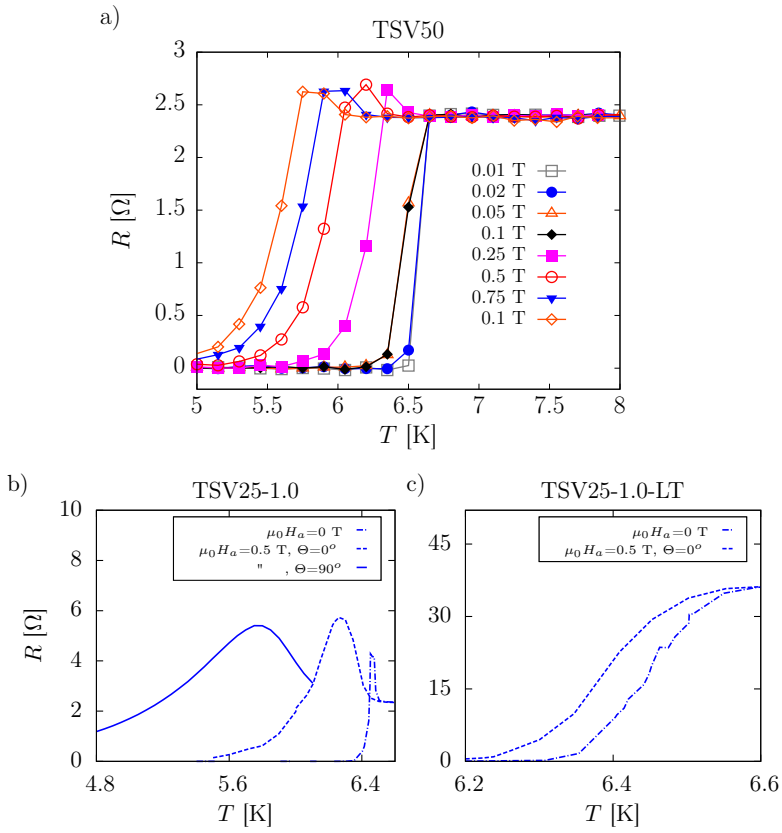

Figure 5.7: (a) Resistive transitions of a spin valve device TSV50a, for different values of the in-plane field between 0 T and 1 T. (b) Transition curves $R(T)$ for a TSV MoGe(25)/Ni(1.5)/Cu(5)/CrO_2(100), at zero field (dot-dash line) and with a field of 0.5 T applied in-plane (dashed line) or out-of-plane (full line); (c) $R(T)$ curves for a TSV with the same characteristics as in a), but with a much lower interface transparency. The dot-dash line is for the measurement at zero field, dashed line for the measurement in-field ($\mu_0 H_a$ = 0.5 T, in-plane).

d_{F_1} = 1.0 nm), where we show the transition curves at zero field and 0.5 T, both in-plane and out-of-plane. The normal state resistance for this structure is about 2.4 Ω. Despite the observed trend, we cannot conclude that there is a connection between superconductor thickness and presence of the peak at zero field. Fig.5.5, for instance, shows a peak at zero field for a TSV with d_S = 50 nm. In general, when present at zero field, the peak is enhanced by the application of a magnetic field.

We believe that the peak is the result of spin accumulation, due to the normal reflection of equal spin triplet Cooper pairs at the half-metallic boundary. As pictorially shown in Fig.5.8, we assume that $m_s = 0$ singlets are converted into $m_s = 0$ triplets in the Ni/Cu sandwich, but that a triplet $m_s = 1$ quantization axis is provided by the misaligned moments, which could be called an F' layer. When these $m_s = 1$ triplets

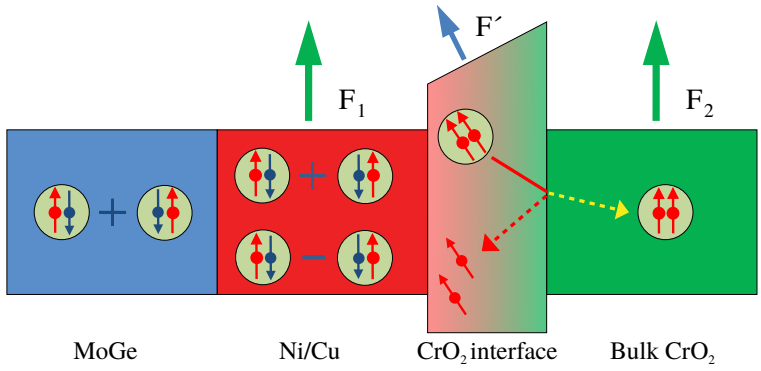

Figure 5.8: Pictorial representation of the effect of an extra ferromagnetic layer F' between the mixer layer F_1 and the drainage layer F_2 on the generation of triplet pairs. The green arrows represent magnetization directions of $F_{1,2}$) (in plane); the blue arrow indicates a interface layer F' with magnetization direction out-of-plane.

encounter the CrO_2 bulk, they will partly be transmitted, but also partly reflected. The latter may result in the breaking of the pair on the MoGe/Cu/Ni-side of the stack, resulting in quasiparticles with the same spin. This spin accumulation raises the spin chemical potential ($\Delta\mu = \mu_\uparrow - \mu_\downarrow$) and results in additional spin contact resistance, which manifests itself as the observed peak at the onset of the superconducting transition. Typically the spin accumulation at the S/F interface is quantified by excess resistance, expressed as

$$\Delta R = \frac{P^2}{1-P^2}\left(\frac{\rho\, l_{sd}}{A}\right), \tag{5.1}$$

where A is the area of the F/S junction, while P, ρ, and l_{sd}, are the spin polarization,

resistivity, and the spin diffusion length of the ferromagnet respectively [27]. This expression cannot be used to quantify ΔR for a half metal as it diverges for $P = 1$, but it is clear that for half metals with P close to 1 the spin accumulation can be considerably larger than in other ferromagnets.

Spin accumulation leads to excess resistance, but that accumulation would occur is non-trivial. The zero-field state can be supposed to generate triplets since the domain state of both ferromagnets can be considered as non-collinear. Applying an in-plane field makes the $F_{1,2}$ magnetizations more collinear, but if the F' magnetization has a component perpendicular to the interface the triplet magnetization axis would indeed be different from the bulk. This can explain the appearance (or the enhancement) of the peak by increasing the field from zero a to a finite (in-plane) value. In the same vein, the effect would be less for the out-of-plane configuration, in which F' and F_2 are becoming more collinear. For devices in which the interface transparency is lower, the peak is not observed. This can be seen in the transitions of Fig.5.7c, for a TSV with the same characteristics as in Fig.5.7b , but with a significantly lower interface transparency, as signaled by the higher R_N value (about 36 Ω). This is on the one hand because of the barrier hindering the proximity with CrO_2 and therefore the polarization, on the other hand because the higher R_N value makes a contribution coming from the spin accumulation less relevant. Theoretical modeling will be needed to investigate the proposed model.

5.3.3 Spin mixer thickness dependence

In this section we present measurements performed on TSV25s with different Ni thickness d_{F_1}, in order to study the dependence and to determine the optimum value. We measured the resistive transition of the TSVs as a function of the temperature, with the magnetic field (0.5 T) applied in-plane ($\theta = 0°$) and out-of-plane ($\theta = 90°$). For simplicity we will call $T_{50\%}$ and $\delta T_{50\%,\max} = T_{50\%}(0°) - T_{50\%}(90°)$ which have been defined above, T_c and δT_c.

In the left panel of Fig.5.9 we plot δT_c as a function of d_{F_1}: as predicted the TSV efficiency shows a strongly non-monotonic behavior with a peak centered around 1.5 nm, which confirms that to be the optimum thickness. For both $d_{F_1} = 0$ nm and $d_{F_1} = 3$ nm, for which no triplet generation is expected, the measured variation $\delta T_c \simeq 350$ mK provides us the magnitude of the triplet-independent effects. We showed that the interface transparency between the CrO_2 film and the trilayer above is a crucial parameter for the injection of the Cooper pairs into the CrO_2 and therefore for the TSV efficiency.

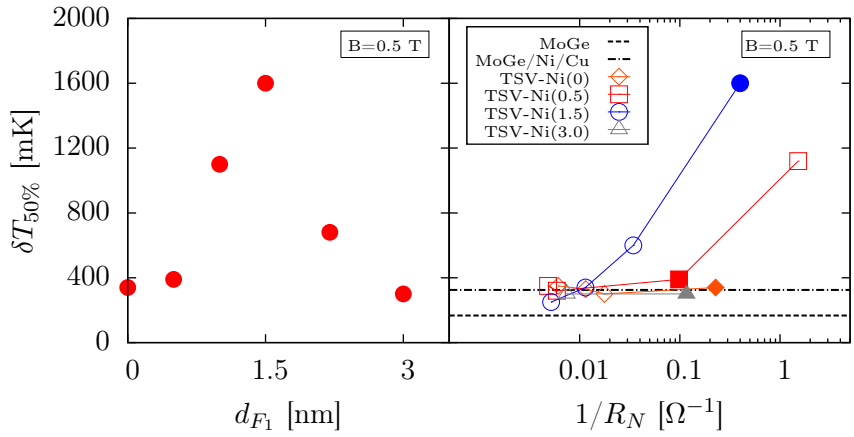

Figure 5.9: (left panel) Dependence of the TSV efficiency, measured by $\delta T_{50\%,\max} = T_{50\%}(0°)$-$T_{50\%}(90°)$ in a field of 0.5 T for TSV25s, as a function of the thickness of the mixer layer d_{F_1} and (right panel) dependence of the TSV efficiency as a function of the interface transparency, measured by the reciprocal of the normal resistance $1/R_N$, for different series of TSV25s, each with a different d_{F_1} value. Dashed and dash-dot lines show the $\delta T_{50\%,\max}$ value for the isolated superconductor MoGe(25) and the trilayer MoGe(25)/Ni(1.5)/Cu(5), respectively. The full symbols represent the points used for the plot in the left panel.

For the TSVs of the left panel of Fig.5.9, the values of R_N are comparable but not fully equal. For this reason, in order to isolate the effect of the variation of the Ni thickness dependence we should compare structures with similar interface transparency, an experimental parameter not controllable with high precision. Nonetheless the differences amongst the TSVs do not change the qualitative behavior presented. This becomes clear in the right panel of Fig.5.9, where the δT_c of different series of TSVs is plotted as function of the interface transparency. Each curve is a series with a different Ni thickness, while the dashed and dash-dot horizontal lines show the T_c variation for a single MoGe(25) layer and a MoGe(25)/Ni(1.5)/Cu(5) trilayer, respectively. The full symbols represent the points used for the plot in the left panel (series Ni(1.0) and Ni (2.2) are not presented for clarity but are consistent with the general behavior). For low transparencies (low $1/R_N$ values) the leakage is suppressed and all the curves approximately converge to the value of the trilayer. Increasing the transparency results in a growing TSV efficiency and the closer the Ni thickness is to the optimum value, the stronger the effect. From the plot it is clear that the TSVs with d_{F_1} = 1.5 nm are the most efficient. This study, not only confirms that the optimum thickness value for the Ni is around 1.5 nm, but also provides a further proof of the spin-triplet origin for the large observed effect.

If we look at the evolution of the peak associated to spin accumulation as function of d_{F_1} (Fig.5.10), we see that the height increases with decreasing the Ni thickness (dashed, full and dash-dot line are for d_{F_1} = 1.0 nm, 1.5 nm and 2.2 nm, respectively). The maximum height/R_N ratio is obtained for the trilayer without nickel (inset). The same trend is observed for the peak at zero field. This is consistent with the spin accumulation mechanism described above: by increasing d_{F_1} we increase the amount of pair-breaking inside the nickel layer so that less and less Cooper pairs reach the interface with CrO_2, decreasing the amount of accumulation. In a trilayer with no Ni layer, triplets can be generated by the non-collinearity between F' and F_2, or simply by the misaligned magnetic moments of the domains of CrO_2, as proposed by previous works [22, 23]. This explains why a peak can be observed also for a trilayer MoGe/Cu/CrO_2, both at zero field and in-field (see inset of Fig.5.10). The properies of F', as well as the interface transparency, are parameters not perfectly controllable. This justify the different behaviors observed for different samples, with regard to peak height or peak evolution from zero field to in-field measurements. In order to achieve a more clear picture about the spin accumulation mechanism further experiments are needed.

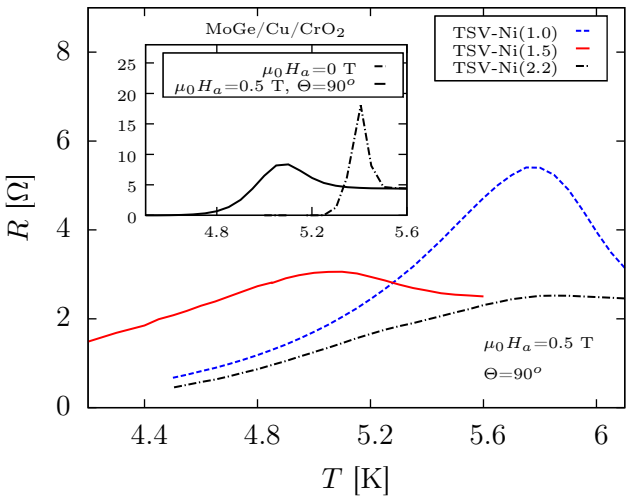

Figure 5.10: Spin accumulation peaks at the onset of the R vs T transition in an out-of-plane field of 0.5 T for TSVs with different Ni layer thickness: 1.0 nm (dashed line), 1.5 nm (full line) and 2.2 nm (dot-dash line). The inset shows the transitions at zero field (dot-dash line) and in-field out-of-plane (full line) for the trilayer MoGe(25)/Cu(5)/CrO_2(100), with no nickel.

5.4 Conclusions

To summarize, we demonstrated a triplet spin valve using a 100 % spin polarized ferromagnet. By changing the field from in-plane to out-of-plane we found very large effects occurring up to magnetic fields of 2 T. The triplet nature of the observed effect is confirmed by the non-monotonic dependence of the TSV efficiency on the thickness of the mixer layer. We also showed that the interface transparency between the bulk magnet and the triplet-generating stack has a decided effect on the efficiency of the TSV. Finally, a characteristic peak in the transition curve of the TSV with the field in plane was explained in terms of spin accumulation caused by equal-spin Cooper pair breaking. We suggest that TSV's, in particular those based on half metals, are good model systems for a systematic study of the parameters which are relevant for triplet generation. We believe that this work will motivate the development of much needed theoretical formalism of TSVs based on half metals[ii].

[ii] After publishing this work [28] a theoretical study on half-metallic TSVs was published by Mironov and Buzdin [29].

BIBLIOGRAPHY

[1] Y. V. Fominov, A. A. Golubov, T. Y. Karminskaya, M. Y. Kupriyanov, R. G. Deminov, and L. R. Tagirov. Superconducting Triplet Spin Valve. *J. Exp. Theor. Phys.* **91**, 308 (2010).

[2] A. K. Feofanov, V. A. Oboznov, V. V. Bol'ginov, J. Lisenfeld, S. Poletto, V. V. Ryazanov, A. N. Rossolenko, M. Khabipov, D. Balashov, A. B. Zorin, P. N. Dmitriev, V. P. Koshelets, and A. V. Ustinov. Implementation of superconductor/ferromagnet/superconductor pi-shifters in superconducting digital and quantum circuits. *Nat. Phys.* **6**, 593 (2010).

[3] H. Enoksen, J. Linder, and A. Sudbo. Pressure-induced 0–π transitions and supercurrent crossover in antiferromagnetic weak links. *Phys. Rev. B* **88**, 214512 (2013).

[4] F. S. Bergeret, A. F. Volkov, and K. B. Efetov. Long-range proximity effects in superconductor-ferromagnet structures. *Phys. Rev. Lett.* **86**, 4096 (2001).

[5] A. Kadigrobov, R. I. Shekhter, and M. Jonson. Quantum spin fluctuations as a source of long-range proximity effects in diffusive ferromagnet-superconductor structures. *Europhys. Lett.* **54**, 394 (2001).

[6] Bergeret, F. S. and Volkov, A. F. and Efetov, K. B. Manifestation of triplet superconductivity in superconductor-ferromagnet structures. *Phys. Rev. B* **68**, 064513 (2003).

[7] M. Houzet and A. I. Buzdin. Long range triplet Josephson effect through a ferromagnetic trilayer. *Phys. Rev. B* **76**, 060504 (2007).

[8] M. Eschrig and T. Loefwander. Triplet supercurrents in clean and disordered half-metallic ferromagnets. *Nat. Phys.* **4**, 138 (2008).

[9] T. S. Khaire, M. A. Khasawneh, W. P. Pratt, Jr., and N. O. Birge. Observation of spin-triplet superconductivity in Co-based Josephson junctions. *Phys. Rev. Lett.* **104**, 137002 (2010).

[10] J. W. A. Robinson, J. D. S. Witt, and M. G. Blamire. Controlled injection of spin-triplet supercurrents into a strong ferromagnet. *Science* **329**, 59 (2010).

[11] M. A. Khasawneh, T. S. Khaire, C. Klose, W. P. P. Jr, and N. O. Birge. Spin-triplet supercurrent in Co-based Josephson junctions. *Supercond. Sci. Technol.* **24**, 024005 (2011).

[12] M. S. Anwar, M. Veldhorst, A. Brinkman, and J. Aarts. Long range supercurrents in ferromagnetic CrO_2 using a multilayer contact structure. *Appl. Phys. Lett.* **100**, 052602 (2012).

[13] C. Klose, T. S. Khaire, Y. Wang, W. P. Pratt, Jr., N. O. Birge, B. J. McMorran, T. P. Ginley, J. A. Borchers, B. J. Kirby, B. B. Maranville, and J. Unguris. Optimization of spin-triplet supercurrent in ferromagnetic Josephson junctions. *Phys. Rev. Lett.* **108**, 127002 (2012).

[14] P. V. Leksin, N. N. Garif'yanov, I. A. Garifullin, Y. V. Fominov, J. Schumann, Y. Krupskaya, V. Kataev, O. G. Schmidt, and B. Buechner. Evidence for triplet superconductivity in a superconductor-ferromagnet spin valve. *Phys. Rev. Lett.* **109**, 057005 (2012).

[15] X. L. Wang, A. Di Bernardo, N. Banerjee, A. Wells, F. S. Bergeret, M. G. Blamire, and J. W. A. Robinson. Giant triplet proximity effect in superconducting pseudo spin valves with engineered anisotropy. *Phys. Rev. B* **89**, 140508 (2014).

[16] N. Banerjee, C. B. Smiet, R. G. J. Smits, A. Ozaeta, F. S. Bergeret, M. G. Blamire, and J. W. A. Robinson. Evidence for spin selectivity of triplet pairs in superconducting spin valves. *Nat. Commun.* **5**, 3048 (2014).

[17] A. A. Jara, C. Safranski, I. N. Krivorotov, C.-T. Wu, A. N. Malmi-Kakkada, O. T. Valls, and K. Halterman. Angular dependence of superconductivity in superconductor/spin-valve heterostructures. *Phys. Rev. B* **89**, 184502 (2014).

[18] M. G. Flokstra, T. C. Cunningham, J. Kim, N. Satchell, G. Burnell, P. J. Curran, S. J. Bending, C. J. Kinane, J. F. K. Cooper, S. Langridge, A. Isidori, N. Pugach, M. Eschrig, and S. L. Lee. Controlled suppression of superconductivity by the generation of polarized Cooper pairs in spin-valve structures. *Phys. Rev. B* **91**, 060501 (2015).

[19] X. W. Li, A. Gupta, and G. Xiao. Influence of strain on the magnetic properties of epitaxial (100) chromium dioxide (CrO_2) films. *Appl. Phys. Lett.* **75**, 713 (1999).

[20] R. S. Keizer. *Singlet and triplet supercurrents in disordered mesoscopic systems.* Ph.D. thesis Delft Technical University (2007).

[21] M. S. Anwar. *Spin triplet supercurrents in thin films of ferromagnetic* CrO_2. Ph.D. thesis.

[22] M. S. Anwar, F. Czeschka, M. Hesselberth, M. Porcu, and J. Aarts. Long-range supercurrents through half-metallic ferromagnetic CrO_2. *Phys. Rev. B* **82**, 100501 (2010).

[23] R. S. Keizer, S. T. B. Goennenwein, T. M. Klapwijk, G. X. Miao, G. Xiao, and A. Gupta. A spin triplet supercurrent through the half-metallic ferromagnet CrO_2. *Nature* **439**, 825 (2006).

[24] Y. V. Fominov, N. M. Chtchelkatchev, and A. A. Golubov. Nonmonotonic critical temperature in superconductor/ferromagnet bilayers. *Phys. Rev. B* **66**, 014507 (2002).

[25] C. Cirillo, S. L. Prischepa, M. Salvato, C. Attanasio, M. Hesselberth, and J. Aarts. Superconducting proximity effect and interface transparency in Nb/PdNi bilayers. *Phys. Rev. B* **72**, 144511 (2005).

[26] G. J. C. van Baarle, A. M. Troianovski, T. Nishizaki, P. H. Kes, and J. Aarts. Imaging of vortex configurations in thin films by scanning-tunneling microscopy. *Appl. Phys. Lett.* **82**, 1081 (2003).

[27] F. J. Jedema, B. J. van Wees, B. H. Hoving, A. T. Filip, and T. M. Klapwijk. Spin-accumulation-induced resistance in mesoscopic ferromagnet-superconductor junctions. *Phys. Rev. B* **60**, 16549 (1999).

[28] A. Singh, S. Voltan, K. Lahabi, and J. Aarts. Colossal proximity effect in a superconducting triplet spin valve based on the half-metallic ferromagnet CrO_2. *Phys. Rev. X* **5**, 021019 (2015).

[29] S. Mironov and A. Buzdin. Triplet proximity effect in superconducting heterostructures with a half-metallic layer. *Phys. Rev. B* **92**, 184506 (2015).